Evaluating the Utility of a Nanoscale Flow Cytometer for Detection of Surface Proteins on HIV and Extracellular Vesicles

Jonathan Burnie[1], Caroline Ouano[1,2], Vanessa Costa[3], Irene Castrosin[3], Catherine Hammond[1,4], Hannah Matthews[1], John Tigges[3,5], Kizzmekia S. Corbett-Helaire[1,4*]

[1]Department of Immunology and Infectious Diseases, Harvard T.H. Chan School of Public Health, Boston, MA, USA

[2]Northeastern University, Boston, MA, USA

[3]Flow Cytometry Core Facility, Beth Israel Deaconess Medical Center, Boston, MA, USA

[4]Howard Hughes Medical Institute, Chevy Chase, MD, USA

[5]Harvard Medical School, Boston, MA, USA

Correspondence: Kizzmekia S. Corbett-Helaire (kizzmekia_corbett@hsph.harvard.edu)

Background: Flow virometry (FV) – the application of flow cytometry to viruses – has historically been hindered by the inability of cytometers to detect particles below ~300 nm in size. However, advances in optics and fluidics have enabled cytometers primarily designed for cells to detect viruses and extracellular vesicles (EVs) through light scatter alone. In 2024, the CytoFLEX nano was released, marketed for the detection of particles as small as 40 nm; however, its performance has yet to be compared to a conventional instrument for FV.

Methods: FV was utilized to evaluate performance of the CytoFLEX nano and a conventional flow cytometer (CytoFLEX S). Instrument scatter sensitivity was assessed using NIST beads (40-400 nm), and virus stocks [human immunodeficiency virus (HIV), human coronaviruses (HCoV)-229E and HCoV-OC43]. For fluorescence analysis, HIV virions were stained with PE- and BV421-conjugated antibodies targeting virion incorporated proteins (CD38, CD44), individually and in combination. Finally, HIV stocks were labeled with antibodies against the envelope (Env) glycoprotein and tetraspanins (CD9, CD81) to assess EVs within virus preparations.

Results: Compared to the CytoFLEX S, the CytoFLEX nano exhibited substantially greater scatter sensitivity, reflected by up to 50-fold higher signal-to-noise ratio across NIST-traceable beads and virus samples. This enabled clearer resolution of smaller populations, including bead populations < 70 nm that were undetectable on the CytoFLEX S, as well as improved resolution across all viruses. While both instruments reliably detected stained proteins on HIV virions, the CytoFLEX nano revealed a distinct population of tetraspanin-positive EVs within HIV stocks that was undetected on the CytoFLEX S. Using GFP-tagged HIV, we identified Env^+ particles lacking GFP, indicating the presence of Env on EVs.

Conclusions: The CytoFLEX nano exhibited markedly improved scatter sensitivity compared to the CytoFLEX S, improving detection of viruses and enabling detection of EV populations that were undetectable on the conventional instrument. While both platforms performed similarly for surface

protein labeling, additional consideration of spectral overlap was needed with the CytoFLEX nano in multicolor experiments. These findings highlight that the complementary strengths of each platform can be utilized to more comprehensively characterize virus and EV populations, providing new opportunities to investigate nanoparticle heterogeneity.

Keywords (3-10): flow virometry, nanoscale flow cytometry, HIV, CytoFLEX S, CytoFLEX nano, virion-incorporated protein

Background

Over the last two decades, the interest in applying flow cytometry to viruses - termed flow virometry (FV)- has become increasingly simple and feasible as cytometry instrumentation has improved (reviewed in[1–4]). FV leverages the quantitative, multiparametric, and high-throughput strengths of flow cytometry, enabling analysis of viruses across diverse applications, including diagnosis and monitoring of viral infections[5–7], characterization of viral heterogeneity[8,9], and for vaccine quality control[10,11]. Detecting viruses directly by light scatter through cytometry has traditionally been challenging since viruses typically fall within the range of instrument background (< 300 nm) on conventional instruments[3,4]. To address this, three common strategies have been routinely employed to permit FV: (1) specialized instrumentation with custom modifications to enhance small particle detection[5,12,13], (2) fluorescent triggering to detect viruses with fluorescent labels (i.e., dyes/fusion proteins)[9,14–22], and (3) bead-based methods that increase light scattering[7,23–26,26–28].

Over the last decade, there has been an emergence of cytometers marketed for cellular analysis that also permit detection of viruses and EVs through light scattering alone[29–37]. Beckman Coulter CytoFLEX instruments (models S and LX) are one such instrument family. These instruments incorporate a series of advancements that facilitate visualization of small particles including avalanche photodiodes, wavelength-division multiplexing, violet scatter detection, and diode lasers to enhance light detection while reducing optical and electronic noise[29]. Using conventional CytoFLEX instruments, FV has previously been used as a tool to study murine leukemia virus[35–39], HIV[8,40–44] and SARS-CoV-2 pseudoviruses[45], largely in the context of evaluating surface proteins without the need for magnetic beads, fluorescent tags, ultracentrifugation, or other auxiliary methods.

In 2024, a new small particle-dedicated instrument (CytoFLEX nano) was released marketed as having technical advancements which specifically facilitate the visualization of smaller particles such as EVs and viruses as small as 40 nm[46]. This enhanced sensitivity is achieved through the use of multiple scatter channels and extended laser dwell times, in addition to other instrument modifications. Notably, while the instrument has already begun being used to analyze the profiles of EVs[47–50], it has yet to be applied to virus labelling. Since surface protein labeling has been well established for HIV on the CytoFLEX S instrument[8,40–44], we selected HIV as a model to compare staining on the conventional CytoFLEX S instrument with the small particle-dedicated nano instrument (CytoFLEX nano).

Herein, we compare the scatter and fluorescence sensitivity of the CytoFLEX nano to the CytoFLEX S for flow virometry assays. We find both instruments readily allow for the detection of single and dual antigens on the HIV surface, demonstrating comparable analytical rigor. However, the CytoFLEX nano offers a

distinct advantage in detecting virions by light scatter with dramatically improved signal-to-noise ratios resulting in an enhanced dynamic range and limit of detection. The CytoFLEX nano also offered additional sensitivity for detecting EVs present within HIV preparations, which were unresolved by the CytoFLEX S. Leveraging this enhanced sensitivity, we probed the presence of tetraspanins as canonical EV markers in HIV stocks to assess the contribution of EVs in these samples. Despite the increased scatter sensitivity, when labeling both tetraspanins and the HIV envelope glycoprotein, we find that the CytoFLEX S enabled a more nuanced analysis of HIV-associated EVs due to an optical configuration which facilitated less spectral spillover. Taken together, we show that both instruments used in tandem can help expand our knowledge of individual virion surfaces.

Methods

Cell culture All cells were grown in a 5% CO_2 humidified incubator at 37 °C in complete media containing 10% FBS (GeminiBio, Cat# 100-106) and 1% penicillin/streptomycin (Life Technologies, Cat# 15140122). HEK293T cells (isolated from a female human embryonic kidney; ATCC, Cat# CRL-11268) were cultured in Dulbecco's modified Eagle's medium (DMEM, Gibco, Cat# 10313-021) while H9 cells (isolated from a 53-year-old male; BEI, Cat# ARP-87) were cultured in RPMI (Gibco, Cat#11875-093).

Virus production Virus production protocols were adapted from previously published methods[8,44]. For infection, H9 cells were pelleted and resuspended in 0.5 mL of undiluted HIV_{IIIB} virus, then incubated for 4 hours at 37 °C. Following infection, fresh media was added, and the cells were transferred to a T75 flask and cultured until the time of harvest (~10-12 days). For virus production via transfection, HEK293T cells were seeded at a density of 0.6×10^5 cells/mL in 6-well plates containing complete media. Transfection was performed once cells reached ~70% confluence. A total of 1 µg of plasmid DNA was used for SG3ΔEnv (ARP-11051) pseudoviruses, and 1.5 µg for HIV iGFP (ARP-12455) and HIV Gag-iGFP JRFL (ARP-12456) viruses. All transfections were conducted using a 1:3 ratio of plasmid DNA (µg) to transfection reagent (µL) (PolyJet™ In Vitro Transfection Reagent, Fisher Scientific, Cat# 50-478-8). Culture supernatants containing virus were collected 48–72 hours post-transfection. All virus stocks were centrifuged at 300 × g for 5 minutes to remove cellular debris before being stored at −80 °C until use.

Monoclonal Antibodies The following antibodies were used for flow virometry staining: PE-conjugated antibodies from BD Biosciences, including CD38 (Cat# 555460), CD44 (Cat# 550989), CD81 (Cat# 555676), and CD9 (Cat# 312106), and from BioLegend, including CD103 (Cat# 350206), CD82 (Cat# 342104), and CD63 (Cat# 353004). The CD103 antibody was used as a negative staining control. BV421-conjugated antibodies were obtained from BD Biosciences for CD81 (Cat# 740079), CD9 (Cat# 743047), and CD63 (Cat# 740080), and from BioLegend for anti-human IgG Fc (Cat#M1310G05), CD38 (Cat# 397120) and CD44 (Cat# 338810). Anti-HIV-1 gp120 Monoclonal Antibody PGT128 (ARP-13352) was obtained from BEI Resources.

Flow virometry staining and CytoFLEX S acquisition Flow virometry was performed using a Beckman Coulter CytoFLEX S equipped with a standard optical configuration. All samples were run for 30 seconds on medium or fast before being recorded for 15 seconds at a sample flow rate of 10 µL/min using the tube loader. Direct and indirect staining protocols were adapted from previously published methods[8,42,44]. For all labeling experiments, cell-free viral supernatants were used at their undiluted titer, with an average particle concentration of ~10^{6-8} particles/mL. For direct labeling, PE- or BV421-conjugated monoclonal

antibodies were used at empirically determined concentrations (0.4–1 µg/mL) and incubated with virus overnight at 4 °C in the dark. For indirect labeling, viruses were incubated overnight at 4 °C in the dark with 0.4 µg/mL of unlabeled PGT128 or isotype control antibody, followed by a 3-hour incubation with 0.5 µg/mL of PE-conjugated secondary antibody (anti-human PE, BioLegend, Cat# 410708). Antibody concentrations were optimized by titration to maximize signal-to-noise ratios (Fig. S1–S4). Following staining, samples were fixed in 2% PFA for 20 minutes. Prior to acquisition, all samples were further diluted in PBS to minimize coincidence.

Fluorescence calibration was performed using ViroCheck NanoParticle Reference Kit (Cat# V10425, Lot# 75221) or BD Quantibrite PE beads (Cat# 340495, Lot# 75221) where indicated. Light scatter calibration was conducted using NIST-traceable size standards (Thermo Fisher Scientific). Calibration was performed using FCM_{PASS} (https://nano.ccr.cancer.gov/fcmpass) as previously described[51]. Additional information on calibration procedures and MIFlowCyt-EV framework controls[52,53] is provided in File S1. Uncalibrated data are shown in arbitrary units (a.u.). Where indicated, calibrated data are shown in estimates of Enveloped Virus (nm) calculated with FCM_{PASS} using the default refractive index (1.456). Flow virometry data were analyzed using FlowJo software (version 10.10.0) and are available on The NanoFlow Repository[54].

CytoFLEX nano flow virometry acquisition Samples were stained as above for the CytoFLEX S and run on the CytoFLEX nano (Beckman Coulter, Brea, CA). The instrument was calibrated through the automated QC and Sensitivity Monitoring performed according to manufacturer's specifications using the CytoFLEX nano Daily QC Scatterspheres, Fluorospheres, and Multi-intensity Fluorospheres (Beckman Coulter, Cat #C85323, #C86350, #C92889). QC values were used to set gains for experimental analysis and confirmed via reference standards (i.e., Exosome standards, fluorescent, Sigma-Aldrich, Cat# SAE0193). Violet-SSC1 (VSSC1-H) trigger was utilized for all data acquisition with a threshold ranging between 325-350. All samples were run at a flow rate of 1 µl/minute. Samples were acquired by time or total number of events as indicated in figure captions. Data analysis and scatter calibration were performed as above. Fluorescence calibration was performed using ViroCheck Nanoparticles.

Results

Comparison of scatter sensitivity for small particle detection. To begin comparing the small particle detection capabilities of the CytoFLEX S and CytoFLEX nano, we first analyzed NIST-traceable 100 nm beads on both instruments. Since this bead population is readily detected by violet side scatter on both platforms, it served as a baseline for comparing signal-to-noise ratios (S/N). By comparing the scatter signals between the bead population and background noise, we found that the signal-to-noise ratio was ~735 on the CytoFLEX nano using the most sensitive violet side scatter channel (VSSCH-1), compared to ~15 on the CytoFLEX S (Fig. 1A). This nearly 50-fold difference demonstrates that the CytoFLEX nano provides substantially greater separation between background noise and specific signal than the conventional instrument.

Next, to assess capabilities of the CytoFLEX nano for small particle detection across a larger scale, we ran a panel of NIST-traceable beads ranging from 40 to 400 nm (Fig. 1B-C). To compare the data on an equivalent scale, we calibrated the FCS files using FCMPass[51] and displayed the data using polystyrene sizing estimates. With the calibrated scale, the beads showed close alignment with the anticipated size for both instruments (Fig. 1B-C). However, the 40, 50 and 70 nm bead populations were unable to be detected

159 on the CytoFLEX S but were detectable on the CytoFLEX nano with the 70 nm population being fully
160 separate from instrument background (Fig. 1C).

161 Since biological samples are known to refract light differently from polystyrene beads due to different
162 refractive indices, we next sought to assess differences in scatter sensitivity across the two instruments
163 using viruses. Since HIV has well established flow virometry protocols[40–44], we used this virus as a reference
164 standard. We additionally tested two human coronaviruses (HCoV-OC43 and HCoV-229E) to extend this
165 analysis to a different class of RNA viruses which commonly circulate as seasonal pathogens. To this end,
166 we ran unstained virus stocks for HIV, HCoV-OC43 and HCoV-229E on both instruments using violet side
167 scatter for visualization (Fig. 1D). Although the CytoFLEX nano is also capable of evaluating scatter using
168 the blue, yellow and red lasers, here analysis was limited to violet side scatter to allow for direct
169 comparison to the CytoFLEX S. As expected, all three viruses – which range in size between ~80-150 nm –
170 were detected on both instruments by side scatter. While the HIV population was clearly resolved from
171 background noise on both platforms, the coronaviruses showed less distinct separation. This suggests that
172 HIV and CoV have differential light scattering properties despite similar sizes. In particular, HCoV-229E
173 overlapped partially with background on the CytoFLEX S but was clearly distinguishable on the CytoFLEX
174 nano (Fig. 1D).

175 Quantitatively, the CytoFLEX nano showed over a 50-fold increase in signal-to-noise ratio for the
176 coronaviruses compared to the conventional CytoFLEX S instrument, similar to the signal-to-noise ratio
177 observed with bead calibration (Fig. 1A), whereas the improvement for HIV was more modest (~30-fold).
178 Attempts to lower the detection threshold on the CytoFLEX S resulted in an increased abort rate and
179 introduced more events attributable to instrument noise and were therefore not pursued. Together, these
180 data indicate that the CytoFLEX nano outperforms the conventional CytoFLEX S instrument in sensitivity
181 for small particle detection, particularly for particles under 100 nm in size.

182

183 **Fluorescent labeling of cellular proteins on HIV virions.** Given the importance of cellular proteins in HIV
184 pathogenesis[55,56], and the existence of established protocols for labeling these proteins on HIV[8,40,41,43,44],
185 we next sought to determine whether the enhanced sensitivity of the CytoFLEX nano provides any
186 advantage over the CytoFLEX S for analyzing virion-incorporated proteins. To this end, we selected the
187 virion-incorporated T-cell antigens CD38[44] and CD44[57] for labeling with PE-conjugated antibodies, since
188 they have previously shown robust staining on virions from the H9 T-cell line using the CytoFLEX S[44]. To
189 assess non-specific antibody labeling, two controls were used: media stained with anti-CD38 and anti-
190 CD44 to measure background signal, and pseudoviruses (SG3 ΔEnv) produced in HEK293T cells lacking the
191 proteins of interest to serve as antigen-specific negative controls.

192 When evaluating CD38 and CD44 staining on the CytoFLEX S, considerable levels of staining on the T-cell-
193 derived virus ($H9_{IIIB}$) were seen as expected, whereas negligible staining was seen on the media,
194 pseudoviruses, and isotype control, (Fig. 2A). On the $H9_{IIIB}$ virus, both cellular proteins were present on
195 two distinct populations within the gated region, suggesting the presence of EVs with the proteins of
196 interest, as seen previously[58]. As expected, the CytoFLEX nano provided a much larger dynamic range for
197 scatter for visualization of smaller particles which are likely attributable to antibody background and

198 labeled EVs (Fig. 2B, far left gate) that were not visible on the CytoFLEX S based on the threshold used
199 (1100). Notably, the CytoFLEX nano provided largely similar fluorescent distributions of the labeled viral
200 populations to those seen with the CytoFLEX S. Of note, when the same sample concentration and
201 acquisition time were used on both instruments, the CytoFLEX S recorded substantially more events than
202 the CytoFLEX nano (Fig. S5). This is likely due in part to the 10-fold higher acquisition rate of the CytoFLEX
203 S compared to the CytoFLEX nano, but may also reflect increased instrument noise on the CytoFLEX S.

204 Although PE fluorescence is often reported in calibrated units of molecules of soluble fluorophore
205 (MESF)[8,40], MESF calibration beads were too large to be acquired on the CytoFLEX nano (~3000 nm).
206 Instead, when we ran Equivalent Reference Fluorophores (ERF) beads dedicated to small particles and
207 compared fluorescence of the $H9_{IIIB}$ samples, we found that the CytoFLEX S displayed higher PE values
208 across all conditions (Fig. 2C). However, it should be mentioned that while the samples were run on the
209 CytoFLEX S at the maximum PE gain, the CytoFLEX nano was run at a considerably lower gain based on the
210 manufacturer's QC guidelines. Thus, it is possible that increased fluorescent signal may have also been
211 possible on the CytoFLEX nano.

212 Both instruments displayed relatively consistent mean fluorescence intensity across a virus dilution series
213 over time (Fig. S6A–D). However, for unstained samples at lower virus concentrations, the CytoFLEX nano
214 showed event counts that more closely aligned with the expected values based on serial dilution (Fig. S6E–
215 H). The CytoFLEX S, however, exhibited increased variability unless stringent cleaning protocols (e.g., PBS
216 or bleach washes) were applied between samples. These cleaning steps were unnecessary for the
217 CytoFLEX nano since it has similar automated steps which occur in between each sample. However, these
218 steps added considerable amounts of time to the acquisition of each sample compared to the CytoFLEX S
219 (45 seconds on the CytoFLEX S vs. 4 minutes on the CytoFLEX nano).

220 **Dual labelling of cellular proteins on HIV.** To assess the capacity of the nano to detect two antigens on the
221 virus surface, we next stained CD38 and CD44 simultaneously on the same samples. For this purpose, we
222 selected BV421 as a secondary fluorophore since it has previously shown to be effective for surface antigen
223 labeling of HIV and MLV using the CytoFLEX S in FV[38,40]. Additionally, we tested both fluorophore-antibody
224 pairings–CD38-PE with CD44-BV421 and CD38-BV421 with CD44-PE–to assess whether the choice of
225 fluorophore affected staining patterns. We observed minimal staining on cell culture media and the
226 negative control viruses, as expected for both instruments (Fig 3A; Fig S7). For $H9_{IIIB}$, staining was seen for
227 both CD38 and CD44 using PE- and BV421-labeled antibodies on the CytoFLEX S, as expected. While PE
228 signals were comparable between the two instruments, the CytoFLEX nano exhibited higher BV421 signal
229 relative to the CytoFLEX S, enabling clearer resolution of stained virus populations. These results
230 demonstrate that the CytoFLEX nano can effectively detect dual antigen labeling on virus particles and
231 may offer modest advantages over the CytoFLEX S in this application.

232

233 **Labelling tetraspanins on HIV preparations.** Since EVs are known to be present in virus preparations and
234 share several surface markers with HIV[59–61], we next sought to evaluate how the CytoFLEX nano could aid
235 in uncovering the presence of EVs in virus preparations. Tetraspanins are a family of transmembrane
236 proteins with a wide range of roles, including regulating cell morphology, motility, invasion and

237 signaling[62,63]. Since tetraspanins such as CD9, CD63 and CD81 are widely recognized as canonical EV
238 markers due to their consistent enrichment on EV membranes[64,65], we sought to test for the presence of
239 these markers on our virus stocks. CD82 was also added to the panel since it is an EV marker[66] that was
240 previously found to be highly abundant in HIV_{IIIB} preparations from H9 cells[44].

241 When stained samples were analyzed using the CytoFLEX S, low levels of CD9 staining were observed in
242 the media-alone condition, likely reflecting EVs from fetal bovine serum (Fig. 4A)[67,68]. Notably, EV marker
243 profiles differed across the viruses: CD9 was detected on HEK293T-derived pseudoviruses (SG3 ΔEnv) but
244 not on T-cell-derived ($H9_{IIIB}$) viruses, where CD9 staining resembled that of the media control. In contrast,
245 CD82 was abundant on H9-derived virions but absent on those from HEK cells, as to be expected based on
246 published data[44]. CD63 and CD81 were detected on both virus types, with CD81 showing particularly
247 strong staining on HEK-derived pseudoviruses.

248 When the same samples were run on the CytoFLEX nano, a secondary scatter population was visualized
249 that was completely unresolved on the CytoFLEX S. While the staining in the virus gate remained largely
250 similar across instruments (Fig. 4B, right gate), staining in the EV gate (Fig. 4B, left gate) revealed that
251 differences exist in the presence of EV populations within the HIV stocks. For instance, while CD63 showed
252 relatively low levels of staining in the virus gate for both viruses, the presence of $CD63^+$ EVs were detected
253 in the pseudovirus sample which were absent in the replication-competent virus sample. Strikingly, a large
254 $CD81^+$ population of EVs were present in the pseudovirus sample that was less abundant in the replication-
255 competent virus. Overall, these findings demonstrate that the CytoFLEX nano enables improved resolution
256 of EV populations within virus preparations that were undetectable using the CytoFLEX S instrument alone.

257

258 **Evaluating the presence of EVs in HIV preparations.** While tetraspanins are known EV markers, they are
259 not exclusive to EVs and can also be present on replication-competent virions[69,70]. To begin addressing the
260 overlap of viruses and EVs in virus preparations, we chose to stain the HIV envelope glycoprotein in tandem
261 with tetraspanins on HIV stocks for testing on both cytometers. For this purpose, we utilized a GFP-
262 expressing recombinant HIV construct which has GFP inserted between the structural proteins capsid and
263 matrix[71]. Thus, the presence of GFP fluorescence in this system is indicative of the viral capsid protein
264 which is more likely to be in abundant in virions compared to EVs.

265 To begin, we stained two virus stocks with the broadly neutralizing anti-Env antibody PGT128[72], using a
266 previously described indirect staining protocol[42]. One virus stock contained a subtype B, R5-tropic
267 envelope from the HIV JR FL strain (iGFP JR FL), while the other was a control virus lacking Env (iGFP ΔEnv).
268 When run on the CytoFLEX S, PGT128 provided robust labeling on the Env^+ virus but not on the ΔEnv virus,
269 as expected. Notably, while the majority of staining was seen on GFP^+ particles (i.e., virus population), a
270 smaller population of Env^+ events were present that did not display GFP, suggesting that these are EVs with
271 HIV Env (Fig. 5A). This was in line with results from Arakelyan *et. al.*, wherein a magnetic nanoparticle-
272 based FV approach was utilized[28].

273 Unfortunately, because the CytoFLEX nano has a co-linear laser detection configuration, it has a higher
274 propensity for spectral overlap than the CytoFLEX S. As a result, when the same samples were run on the

275 CytoFLEX nano, all GFP$^+$ events were also positive in the PE channel without compensation, impacting
276 detection of Env which was also detected in the PE channel (Fig. 5A). Despite this, a clear difference in
277 staining was still seen on the CytoFLEX nano for Env staining on the Env$^+$ and ΔEnv viruses.

278 Next, we performed tetraspanin staining on the same GFP-tagged virus stocks, focusing on CD9 and CD81
279 as representative tetraspanins of low and high abundance on HEK cell-derived viruses, respectively (Fig.
280 4). When analyzed on the CytoFLEX S, two distinct positive populations were observed for both CD9 and
281 CD81: one GFP$^+$ and one GFP$^-$(Fig. 5B). This finding aligns with our prior CytoFLEX nano results, which
282 revealed a distinct EV population within HIV preparations expressing these tetraspanins (Fig. 4B). While
283 the same populations were present on the CytoFLEX nano, the enhanced BV421 signal from the CytoFLEX
284 nano resulted in a distribution that was different from the S, indicative of spectral spillover.

285 Finally, we stained both Env and tetraspanins on the virus preparations. On the CytoFLEX S, clear Env$^+$ and
286 tetraspanin-positive populations were present on the JR FL Env virus but not the ΔEnv control, as expected
287 (Fig. 5C). For both CD9$^-$ and CD81$^-$ labeled samples we saw three distinct populations within HIV stocks: (1)
288 virions bearing Env and tetraspanins, (2) virions with Env that lack tetraspanins, and (3) EVs bearing
289 tetraspanins but lacking Env. On the CytoFLEX nano, while the same populations were seen, spillover
290 between GFP from the viruses and PE from Env staining resulted in all GFP$^+$ viruses being detected as PE
291 positive. Thus, while both instruments allow for multicolor labeling, compensation is more likely to be
292 required on the CytoFLEX nano, even for color combinations that did not require compensation on the S.

293

294 **Discussion**

295 While detection of unlabeled virions was previously challenging on conventional cytometers due to
296 instrument limitations[1,3,4], newer instruments have made flow virometry an increasingly accessible tool
297 for single-virion characterization. Here, we demonstrated that while conventional cytometers like the
298 CytoFLEX S provide strong utility for evaluating surface proteins on HIV, small particle-dedicated
299 instruments, such as the CytoFLEX nano, offer clear advantages for analyzing viruses and EVs under 120
300 nm. The most notable difference between the instruments was scatter sensitivity, where the CytoFLEX
301 nano provided dramatically improved signal-to-noise ratios and enabled detection of populations entirely
302 undetectable on the CytoFLEX S. This enhanced resolution is particularly relevant given the growing
303 interest in virus-associated EVs and their potential roles in infection[28,73–75].

304 While the CytoFLEX nano performed relatively comparably to the CytoFLEX S for labeling surface antigens
305 such as CD38 and CD44 on HIV virions, it did not exhibit notable improvements in fluorescence sensitivity
306 in the PE channel. This is notable, as PE is commonly used for flow virometry[8,36–44] because its intrinsic
307 properties (size and brightness), together with the availability of reference materials, make it well suited
308 for quantitative labeling of surface proteins[76,77].

309 Importantly, although CD38 and CD44 were abundant in the virions analyzed here, many relevant viral
310 proteins are expressed at much lower levels[37,55,56,78]. Thus, enhanced fluorescence sensitivity remains a
311 key need for future instruments to enable reliable detection of low abundance viral surface proteins[1].
312 Additionally, we observed differences in virus staining profiles when labeling the same antigen with PE

313 versus BV421, despite both being considered bright fluorophores in cellular flow cytometry. This highlights
314 the potential to further optimize brighter fluorophores specifically engineered for small particle
315 applications to maximize detection of low abundance antigens.

316 The ability to distinguish virions from EVs remains a critical hurdle in the field due to the overlapping size
317 range (~100-120 nm), biogenesis pathways, and shared surface markers[60,61]. Leveraging enhanced scatter
318 sensitivity of the CytoFLEX nano, we detected EVs in HIV stocks with scatter and antigenic signatures
319 distinct from virions. We hypothesize these EVs are most likely to be exosomes (30–150 nm) and
320 microvesicles (50–1000 nm) due to their size ranges which overlap with those of HIV[79–81]. However, as EV
321 biology and cytometric technologies continue to advance, future work should entail more detailed
322 discrimination of the specific populations of EVs that exist within virus preparations. Previously, Arakelyan
323 *et al.* showed that Env was present on HIV-associated EVs by using a magnetic nanoparticle-based flow
324 virometry approach[28]. Our result shows that improvements in flow cytometry instrumentation can
325 facilitate more precise visualization of Env on EVs without the requirement of magnetic nanoparticles. In
326 this study, we also utilized an infectious molecular clone with structural proteins that are GFP-tagged[71] to
327 distinguish between virions and EVs. However, developing protocols that enable internal staining of capsid
328 proteins in wild-type virions would further enhance the power of small particle cytometry for
329 characterizing EV content in viral preparations.

330 Despite the increased scatter sensitivity of the CytoFLEX nano, we found that the conventional instrument
331 remained better suited in some key areas for flow virometry. For instance, the altered optical figuration
332 on the CytoFLEX nano resulted in increased spectral overlap, particularly between GFP and PE channels
333 and GFP and BV421 channels, which impacted dual labeling experiments targeting the HIV Env and
334 tetraspanins. In contrast, the CytoFLEX S provided more distinct spectral separation for multicolor analysis.
335 Moreover, while the CytoFLEX nano allowed for increased sensitivity, this is partially achieved by a ten-
336 fold reduction in the sample flow rate (1 µl/min vs 10 µl/min) and automated cleaning protocols which are
337 run between each sample. These features increase overall experimental acquisition length, reducing the
338 capacity for high throughput applications. Thus, rather than a replacement for conventional instruments,
339 the CytoFLEX nano can complement existing platforms with its distinct strengths for small particle analysis.
340 Of note, although many FV studies omit wash steps to remove unbound antibodies[8,37–44], the increased
341 sensitivity of the CytoFLEX nano allowed for visualization of antibody aggregates in our flow plots,
342 highlighting the need for careful antibody titration to minimize non-specific signal.

343 While virus sorting was not performed in this study, integrating it with the enhanced scatter sensitivity of
344 the CytoFLEX nano could enable more detailed analysis of viral heterogeneity and the high proportion of
345 defective particles within virus stocks – a feature especially prominent in HIV, where most virions produced
346 during infection are non-infectious[82].

347 **Conclusions**

348 In this study, we demonstrate that the CytoFLEX nano is comparable to the CytoFLEX S for phenotyping
349 HIV surface proteins using established surface staining protocols. However, the CytoFLEX nano exhibited
350 markedly improved sensitivity for detecting small particles by light scatter. This improved light scatter
351 sensitivity revealed vesicle populations within HIV stocks that were undetectable on the CytoFLEX S,

352 offering new opportunities to investigate virus-vesicle heterogeneity. However, spectral spillover on the
353 CytoFLEX nano limits its suitability for complex multicolor analyses, and lengthy sample loading times
354 reduce its utility for high-throughput applications. These results highlight the value of leveraging both
355 platforms to achieve a fuller and more nuanced understanding of virus and vesicle populations.

356 **Declarations**

357 **Ethics approval and consent to participate.** Not applicable.

358 **Consent for publication.** All authors approved the manuscript for publication.

359 **Competing interests.** John Tigges consults for Beckman Coulter. All other authors declare no competing
360 interests.

361 **Availability of data and materials**. Source data supporting the findings of this study are available within
362 this paper and its supplementary files. All FCS files are available on nano flow repository ID# 4851013737.
363 Additional source data and materials inquiries should be directed to the corresponding author, Kizzmekia
364 Corbett-Helaire (kizzmekia_corbett@hsph.harvard.edu). Materials will be made available after
365 completion of a Material Transfer Agreement (MTA). If the material was obtained under use restriction,
366 the inquiry will be forwarded to appropriate party.

367 **Funding.** This work was supported, in part, by Chan Zuckerberg Initiative Science Diversity Leadership
368 grant (No. 2022-310965 to KSC), Howard Hughes Medical Institute Freeman Hrabowski Scholars grant (to
369 KSC), start-up funds from Harvard T.H. Chan School of Public Health (to KSC), in-kind gifts of lab
370 equipment, consumables, and supplies from Corning, Inc. (to KSC). JB is supported by a REDI fellowship
371 funded by the Canadian Institutes of Health Research (CIHR-ED6 190739).

372

373 **Author Contributions:** Conceptualization – JB, VC, JT; Investigation – JB, CO, VC, IC, GH, HM, CH; Resources
374 – JT, KSC; Supervision – JT, KSC; Writing (original draft) – JB; Writing (review & editing) – all authors.

375 **Acknowledgments:** We thank Fidan Baycora for administrative support and Emily Hobbs for grant
376 support. Reagents were obtained through the BEI Resources, National Institutes of Allergy and Infectious
377 Diseases, National Institutes of Health: H9 Cells, ARP-87; HIV-1 Non-Infectious Molecular Clone NL4-3 Gag-
378 iGFP ΔEnv (ARP-12455), contributed by Dr. Benjamin K. Chen; Anti-HIV-1 gp120 Monoclonal Antibody
379 PGT128 (ARP-13352), contributed by the International AIDS Vaccine Initiative; HIV-1 SG3ΔEnv (ARP-
380 11051), contributed by Dr. John C. Kappes and Dr. Christina Ochsenbauer; and HIV-1 Gag-iGFP JRFL (ARP-
381 12456), contributed by Dr. Benjamin K. Chen. We thank BioLegend for providing the CD38 and CD44 PE-
382 labeled antibodies. During the preparation of this work, JB used ChatGPT version 5.2 in order to edit and
383 enhance readability of the text. After using this tool, the authors reviewed and edited the content and
384 take full responsibility for the content.
385

386 **List of abbreviations**
387

388 a.u. – arbitrary units; PE – Phycoerythrin; MESF – Molecules of Equivalent Soluble Fluorochrome; HIV –
389 Human Immunodeficiency Virus; HCoV – Human Coronavirus; FBS – Fetal Bovine Serum; FV – Flow

390 Virometry; ERF – Equivalent Reference Fluorophores; EV – Extracellular Vesicle; Env – Envelope
391 Glycoprotein; MFI – Median Fluorescence Intensity; SSC – Side Scatter; S/N – Signal-to-noise ratio.

392

393 **References**

394 1. Fernandes C, Persaud AT, Chaphekhar D, et al. Flow virometry: recent advancements, best practices,
395 and future frontiers. *J Virol*. 2025;99(2):e01717-24. doi:10.1128/jvi.01717-24

396 2. Zamora JLR, Aguilar HC. Flow virometry as a tool to study viruses. *Methods*. 2018;134-135:87-97.
397 doi:10.1016/j.ymeth.2017.12.011

398 3. Lippé R. Flow Virometry: a Powerful Tool To Functionally Characterize Viruses. *J Virol*.
399 2018;92(3):10.1128/jvi.01765-17. doi:10.1128/jvi.01765-17

400 4. Tabler CO, Tilton JC. Analysis of Individual Viral Particles by Flow Virometry. *Viruses*. 2024;16(5):802.
401 doi:10.3390/v16050802

402 5. Hussain R, Ongaro AE, Concepción MLR de la, et al. Small form factor flow virometer for SARS-CoV-2.
403 *Biomed Opt Express*. 2022;13(3):1609-1619. doi:10.1364/BOE.450212

404 6. Soni N, Pai P, Krishna Kumar GR, Prasad V, Dasgupta S, Bhadra B. A Flow Virometry Process Proposed
405 for Detection of SARS-CoV-2 and large-scale Screening of COVID-19 Cases. *Future Virol*.
406 2020;15(8):525-532. doi:10.2217/fvl-2020-0141

407 7. Samman N, El-Boubbou K, Al-Muhalhil K, et al. MICaFVi: A Novel Magnetic Immuno-Capture Flow
408 Virometry Nano-Based Diagnostic Tool for Detection of Coronaviruses. *Biosensors*. 2023;13(5):553.
409 doi:10.3390/bios13050553

410 8. Burnie J, Persaud AT, Thaya L, et al. P-selectin glycoprotein ligand-1 (PSGL-1/CD162) is incorporated
411 into clinical HIV-1 isolates and can mediate virus capture and subsequent transfer to permissive cells.
412 *Retrovirology*. 2022;19(1):9. doi:10.1186/s12977-022-00593-5

413 9. El Bilali N, Duron J, Gingras D, Lippé R. Quantitative Evaluation of Protein Heterogeneity within
414 Herpes Simplex Virus 1 Particles. *J Virol*. 2017;91(10):e00320-17. doi:10.1128/JVI.00320-17

415 10. Yi S, McCracken R, Davide J, et al. Development of process analytical tools for rapid monitoring of
416 live virus vaccines in manufacturing. *Sci Rep*. 2022;12(1):15494. doi:10.1038/s41598-022-19744-x

417 11. Ricci G, Minsker K, Kapish A, et al. Flow virometry for process monitoring of live virus vaccines-
418 lessons learned from ERVEBO. *Sci Rep*. 2021;11(1):7432. doi:10.1038/s41598-021-86688-z

419 12. Hercher M, Mueller W, Shapiro HM. Detection and discrimination of individual viruses by flow
420 cytometry. *J Histochem Cytochem*. 1979;27(1):350-352. doi:10.1177/27.1.374599

421 13. Gaudin R, Barteneva NS. Sorting of small infectious virus particles by flow virometry reveals distinct
422 infectivity profiles. *Nat Commun*. 2015;6:6022. doi:10.1038/ncomms7022

14. Brussaard CPD. Optimization of Procedures for Counting Viruses by Flow Cytometry. *Appl Environ Microbiol*. 2004;70(3):1506-1513. doi:10.1128/AEM.70.3.1506-1513.2004

15. Marie D, Brussaard CPD, Thyrhaug R, Bratbak G, Vaulot D. Enumeration of Marine Viruses in Culture and Natural Samples by Flow Cytometry. *APPL Env MICROBIOL*. 1999;65:8.

16. Brussaard CPD, Marie D, Bratbak G. Flow cytometric detection of viruses. *J Virol Methods*. 2000;85(1):175-182. doi:10.1016/S0166-0934(99)00167-6

17. Khalil JYB, Langlois T, Andreani J, et al. Flow Cytometry Sorting to Separate Viable Giant Viruses from Amoeba Co-culture Supernatants. *Front Cell Infect Microbiol*. 2017;6:202. doi:10.3389/fcimb.2016.00202

18. Khalil JYB, Robert S, Reteno DG, Andreani J, Raoult D, La Scola B. High-Throughput Isolation of Giant Viruses in Liquid Medium Using Automated Flow Cytometry and Fluorescence Staining. *Front Microbiol*. 2016;7:26. doi:10.3389/fmicb.2016.00026

19. Khadivjam B, El Bilali N, Lippé R. Analysis and Sorting of Individual HSV-1 Particles by Flow Virometry. In: Diefenbach RJ, Fraefel C, eds. *Herpes Simplex Virus : Methods and Protocols*. Springer; 2020:289-303. doi:10.1007/978-1-4939-9814-2_16

20. Loret S, El Bilali N, Lippé R. Analysis of herpes simplex virus type I nuclear particles by flow cytometry. *Cytometry A*. 2012;81A(11):950-959. doi:10.1002/cyto.a.22107

21. Bonar MM, Tilton JC. High sensitivity detection and sorting of infectious human immunodeficiency virus (HIV-1) particles by flow virometry. *Virology*. 2017;505:80-90. doi:10.1016/j.virol.2017.02.016

22. Bonar MM, Tabler CO, Haqqani AA, et al. Nanoscale flow cytometry reveals interpatient variability in HIV protease activity that correlates with viral infectivity and identifies drug-resistant viruses. *Sci Rep*. 2020;10(1):18101. doi:10.1038/s41598-020-75118-1

23. Arakelyan A, Fitzgerald W, Margolis L, Grivel JC. Nanoparticle-based flow virometry for the analysis of individual virions. *J Clin Invest*. 2013;123(9):3716-3727. doi:10.1172/JCI67042

24. Zicari S, Arakelyan A, Fitzgerald W, et al. Evaluation of the maturation of individual Dengue virions with flow virometry. *Virology*. 2016;488:20-27. doi:10.1016/j.virol.2015.10.021

25. Arakelyan A, Petersen JD, Blazkova J, Margolis L. Macrophage-derived HIV-1 carries bioactive TGF-beta. *Sci Rep*. 2019;9(1):1. doi:10.1038/s41598-019-55615-8

26. Yan X, Schielke EG, Grace KM, Hassell C, Marrone BL, Nolan JP. Microsphere-based duplexed immunoassay for influenza virus typing by flow cytometry. *J Immunol Methods*. 2004;284(1):27-38. doi:10.1016/j.jim.2003.09.016

27. Samman N, Aljami HA, Alhayli S, et al. Implementation and validation of MICaFVi: A highly efficient nanotechnology-based method for coronaviruses detection. *Sens Actuators Rep*. 2024;8:100248. doi:10.1016/j.snr.2024.100248

457 28. Arakelyan A, Fitzgerald W, Zicari S, Vanpouille C, Margolis L. Extracellular Vesicles Carry HIV Env and
458 Facilitate Hiv Infection of Human Lymphoid Tissue. *Sci Rep*. 2017;7:1695. doi:10.1038/s41598-017-
459 01739-8

460 29. Brittain GC, Chen YQ, Martinez E, et al. A Novel Semiconductor-Based Flow Cytometer with
461 Enhanced Light-Scatter Sensitivity for the Analysis of Biological Nanoparticles. *Sci Rep*. 2019;9:16039.
462 doi:10.1038/s41598-019-52366-4

463 30. Morales-Kastresana A, Telford B, Musich TA, et al. Labeling extracellular vesicles for nanoscale flow
464 cytometry. *Sci Rep*. 2017;7(1):1878.

465 31. Morales-Kastresana A, Musich TA, Welsh JA, et al. High-fidelity detection and sorting of nanoscale
466 vesicles in viral disease and cancer. *J Extracell Vesicles*. 2019;8(1):1597603.
467 doi:10.1080/20013078.2019.1597603

468 32. Sharma M, Sheth M, Poling HM, Kuhnell D, Langevin SM, Esfandiari L. Rapid purification and
469 multiparametric characterization of circulating small extracellular vesicles utilizing a label-free lab-
470 on-a-chip device. *Sci Rep*. 2023;13(1):1. doi:10.1038/s41598-023-45409-4

471 33. O'Leary M, L. Bowtell J, Richards M, et al. Effects of the DailyColors™ polyphenol supplement on
472 serum proteome, cognitive function, and health in older adults at risk of cognitive and functional
473 decline. *Food Funct*. Published online 2025. doi:10.1039/D4FO06259K

474 34. Cook S, Tang VA, Lannigan J, Jones JC, Welsh JA. Quantitative flow cytometry enables end-to-end
475 optimization of cross-platform extracellular vesicle studies. *Cell Rep Methods*. 2023;3(12).
476 doi:10.1016/j.crmeth.2023.100664

477 35. Renner TM, Tang VA, Burger D, Langlois MA. Intact Viral Particle Counts Measured by Flow Virometry
478 Provide Insight into the Infectivity and Genome Packaging Efficiency of Moloney Murine Leukemia
479 Virus. *J Virol*. 2020;94(2):10.1128/jvi.01600-19. doi:10.1128/jvi.01600-19

480 36. Welsh JA, Jones JC, Tang VA. Fluorescence and Light Scatter Calibration Allow Comparisons of Small
481 Particle Data in Standard Units across Different Flow Cytometry Platforms and Detector Settings.
482 *Cytometry A*. 2020;97(6):592-601. doi:10.1002/cyto.a.24029

483 37. Maltseva M, Langlois MA. Influence of GlycoGag on the Incorporation of Host Membrane Proteins
484 Into the Envelope of the Moloney Murine Leukemia Virus. *Front Virol*. 2021;1.
485 doi:10.3389/fviro.2021.747253

486 38. Tang VA, Fritzsche AK, Renner TM, et al. Engineered Retroviruses as Fluorescent Biological Reference
487 Particles for Small Particle Flow Cytometry. *bioRxiv*. Preprint posted online June 7, 2019:614461.
488 doi:10.1101/614461

489 39. Maltseva M, Langlois MA. Flow Virometry for Characterizing the Size, Concentration, and Surface
490 Antigens of Viruses. *Curr Protoc*. 2022;2(2):e368. doi:10.1002/cpz1.368

491 40. Burnie J, Tang VA, Welsh JA, et al. Flow Virometry Quantification of Host Proteins on the Surface of
492 HIV-1 Pseudovirus Particles. *Viruses*. 2020;12(11):11. doi:10.3390/v12111296

41. Persaud AT, Khela J, Fernandes C, et al. Virion-incorporated CD14 enables HIV-1 to bind LPS and initiate TLR4 signaling in immune cells. *J Virol*. 98(5):e00363-24. doi:10.1128/jvi.00363-24

42. Burnie J, Fernandes C, Patel A, et al. Applying Flow Virometry to Study the HIV Envelope Glycoprotein and Differences Across HIV Model Systems. *Viruses*. 2024;16(6):6. doi:10.3390/v16060935

43. Chaphekar D, Fernandes C, Persaud AT, Guzzo C. Comparing methods to detect cellular proteins on the surface of HIV-1 virions. *J Virol Methods*. Published online December 6, 2024:115096. doi:10.1016/j.jviromet.2024.115096

44. Burnie J, Fernandes C, Chaphekar D, et al. Identification of CD38, CD97, and CD278 on the HIV surface using a novel flow virometry screening assay. *Sci Rep*. 2023;13(1):23025. doi:10.1038/s41598-023-50365-0

45. Maltseva M, Rossotti MA, Tanha J, Langlois MA. Characterization of Nanobody Binding to Distinct Regions of the SARS-CoV-2 Spike Protein by Flow Virometry. *Viruses*. 2025;17(4):4. doi:10.3390/v17040571

46. Application Note: CytoFLEX nano Flow Cytometer: the new frontier of nanoscale Flow Cytometry. Accessed January 22, 2025. https://www.nature.com/articles/d42473-024-00117-z

47. Lin YH, Chen Y, Liu EW, et al. Immunomodulation effects of collagen hydrogel encapsulating extracellular vesicles derived from calcium silicate stimulated-adipose mesenchymal stem cells for diabetic healing. *J Nanobiotechnology*. 2025;23(1):45. doi:10.1186/s12951-025-03097-4

48. Chen YW, Lin YH, Ho CC, et al. High-yield extracellular vesicle production from HEK293T cells encapsulated in 3D auxetic scaffolds with cyclic mechanical stimulation for effective drug carrier systems. *Biofabrication*. 2024;16(4):045035. doi:10.1088/1758-5090/ad728b

49. Gudbergsson JM, Malle MG, Jensen JB, et al. Dedicated nanoparticle flow cytometry for single extracellular vesicle phenotyping: Performance of the CytoFLEX Nano. *bioRxiv*. Preprint posted online December 17, 2025:2025.12.15.694348. doi:10.64898/2025.12.15.694348

50. Cao L, Wang H, Zhu J, et al. Exploring exosome profiling via CytoFLEX Nano flow cytometer: Approaches and applications. *VIEW*. 2025;6(6):20250068. doi:10.1002/VIW.20250068

51. Welsh JA, Jones JC. Small Particle Fluorescence and Light Scatter Calibration Using FCMPASS Software. *Curr Protoc Cytom*. 2020;94(1):e79. doi:10.1002/cpcy.79

52. Welsh JA, Arkesteijn GJA, Bremer M, et al. A compendium of single extracellular vesicle flow cytometry. *J Extracell Vesicles*. 2023;12(2):e12299. doi:10.1002/jev2.12299

53. Welsh JA, Van Der Pol E, Arkesteijn GJA, et al. MIFlowCyt-EV: a framework for standardized reporting of extracellular vesicle flow cytometry experiments. *J Extracell Vesicles*. 9(1):1713526. doi:10.1080/20013078.2020.1713526

54. Arce JE, Welsh JA, Cook S, et al. The NanoFlow Repository. *Bioinformatics*. 2023;39(6):btad368. doi:10.1093/bioinformatics/btad368

529 55. Burnie J, Guzzo C. The Incorporation of Host Proteins into the External HIV-1 Envelope. *Viruses*.
530 2019;11(1):85. doi:10.3390/v11010085

531 56. Tremblay MJ, Fortin JF, Cantin R. The acquisition of host-encoded proteins by nascent HIV-1.
532 *Immunol Today*. 1998;19(8):346-351. doi:10.1016/S0167-5699(98)01286-9

533 57. ORENTAS RJ, HILDRETH JEK. Association of Host Cell Surface Adhesion Receptors and Other
534 Membrane Proteins with HIV and SIV. *AIDS Res Hum Retroviruses*. 1993;9(11):1157-1165.
535 doi:10.1089/aid.1993.9.1157

536 58. Cantin R, Diou J, Bélanger D, Tremblay AM, Gilbert C. Discrimination between exosomes and HIV-1:
537 Purification of both vesicles from cell-free supernatants. *J Immunol Methods*. 2008;338(1):21-30.
538 doi:10.1016/j.jim.2008.07.007

539 59. Moulin C, Crupi MJF, Ilkow CS, Bell JC, Boulton S. Extracellular Vesicles and Viruses: Two Intertwined
540 Entities. *Int J Mol Sci*. 2023;24(2):2. doi:10.3390/ijms24021036

541 60. Nolte-'t Hoen E, Cremer T, Gallo RC, Margolis LB. Extracellular vesicles and viruses: Are they close
542 relatives? *Proc Natl Acad Sci*. 2016;113(33):9155-9161. doi:10.1073/pnas.1605146113

543 61. Gould SJ, Booth AM, Hildreth JEK. The Trojan exosome hypothesis. *Proc Natl Acad Sci*.
544 2003;100(19):10592-10597. doi:10.1073/pnas.1831413100

545 62. Hemler ME. Tetraspanin functions and associated microdomains. *Nat Rev Mol Cell Biol*.
546 2005;6(10):801-811. doi:10.1038/nrm1736

547 63. Charrin S, Jouannet S, Boucheix C, Rubinstein E. Tetraspanins at a glance. *J Cell Sci*.
548 2014;127(17):3641-3648. doi:10.1242/jcs.154906

549 64. Rubinstein E, Théry C, Zimmermann P. Tetraspanins affect membrane structures and the trafficking
550 of molecular partners: what impact on extracellular vesicles? *Biochem Soc Trans*. 2025;53(02):371-
551 382. doi:10.1042/BST20240523

552 65. Willms E, Cabañas C, Mäger I, Wood MJA, Vader P. Extracellular Vesicle Heterogeneity:
553 Subpopulations, Isolation Techniques, and Diverse Functions in Cancer Progression. *Front Immunol*.
554 2018;9. doi:10.3389/fimmu.2018.00738

555 66. Jankovičová J, Sečová P, Michalková K, Antalíková J. Tetraspanins, More than Markers of Extracellular
556 Vesicles in Reproduction. *Int J Mol Sci*. 2020;21(20):7568. doi:10.3390/ijms21207568

557 67. Lehrich BM, Liang Y, Fiandaca MS. Foetal bovine serum influence on in vitro extracellular vesicle
558 analyses. *J Extracell Vesicles*. 2021;10(3):e12061. doi:10.1002/jev2.12061

559 68. Urzì O, Olofsson Bagge R, Crescitelli R. The dark side of foetal bovine serum in extracellular vesicle
560 studies. *J Extracell Vesicles*. 2022;11(10):e12271. doi:10.1002/jev2.12271

561 69. Jolly C, Sattentau QJ. Human Immunodeficiency Virus Type 1 Assembly, Budding, and Cell-Cell
562 Spread in T Cells Take Place in Tetraspanin-Enriched Plasma Membrane Domains. *J Virol*.
563 2007;81(15):7873-7884. doi:10.1128/JVI.01845-06

564 70. Ruiz-Mateos E, Pelchen-Matthews A, Deneka M, Marsh M. CD63 Is Not Required for Production of
565 Infectious Human Immunodeficiency Virus Type 1 in Human Macrophages. *J Virol*.
566 2008;82(10):4751-4761. doi:10.1128/jvi.02320-07

567 71. Hübner W, Chen P, Portillo AD, Liu Y, Gordon RE, Chen BK. Sequence of Human Immunodeficiency
568 Virus Type 1 (HIV-1) Gag Localization and Oligomerization Monitored with Live Confocal Imaging of a
569 Replication-Competent, Fluorescently Tagged HIV-1. *J Virol*. 2007;81(22):12596-12607.
570 doi:10.1128/JVI.01088-07

571 72. Pejchal R, Doores KJ, Walker LM, et al. A potent and broad neutralizing antibody recognizes and
572 penetrates the HIV glycan shield. *Science*. 2011;334(6059):1097-1103. doi:10.1126/science.1213256

573 73. Bello-Morales R, Ripa I, López-Guerrero JA. Extracellular Vesicles in Viral Spread and Antiviral
574 Response. *Viruses*. 2020;12(6):623. doi:10.3390/v12060623

575 74. DeMarino C, Denniss J, Cowen M, et al. HIV-1 RNA in extracellular vesicles is associated with
576 neurocognitive outcomes. *Nat Commun*. 2024;15(1):4391. doi:10.1038/s41467-024-48644-z

577 75. Giannessi F, Aiello A, Franchi F, Percario ZA, Affabris E. The Role of Extracellular Vesicles as Allies of
578 HIV, HCV and SARS Viruses. *Viruses*. 2020;12(5):571. doi:10.3390/v12050571

579 76. Schwartz A, Wang L, Early E, et al. Quantitating Fluorescence Intensity from Fluorophore: The
580 Definition of MESF Assignment. *J Res Natl Inst Stand Technol*. 2002;107(1):83-91.
581 doi:10.6028/jres.107.009

582 77. Wang L, Gaigalas AK, Abbasi F, Marti GE, Vogt RF, Schwartz A. Quantitating Fluorescence Intensity
583 From Fluorophores: Practical Use of MESF Values. *J Res Natl Inst Stand Technol*. 2002;107(4):339-
584 353. doi:10.6028/jres.107.027

585 78. Guzzo C, Ichikawa D, Park C, et al. Virion incorporation of integrin α4β7 facilitates HIV-1 infection and
586 intestinal homing. *Sci Immunol*. 2017;2(11):eaam7341. doi:10.1126/sciimmunol.aam7341

587 79. van Niel G, D'Angelo G, Raposo G. Shedding light on the cell biology of extracellular vesicles. *Nat Rev*
588 *Mol Cell Biol*. 2018;19(4):213-228. doi:10.1038/nrm.2017.125

589 80. Doyle LM, Wang MZ. Overview of Extracellular Vesicles, Their Origin, Composition, Purpose, and
590 Methods for Exosome Isolation and Analysis. *Cells*. 2019;8(7):727. doi:10.3390/cells8070727

591 81. Sheta M, Taha EA, Lu Y, Eguchi T. Extracellular Vesicles: New Classification and Tumor
592 Immunosuppression. *Biology*. 2023;12(1):110. doi:10.3390/biology12010110

593 82. Finzi D, Plaeger SF, Dieffenbach CW. Defective Virus Drives Human Immunodeficiency Virus Infection,
594 Persistence, and Pathogenesis. *Clin Vaccine Immunol*. 2006;13(7):715-721. doi:10.1128/CVI.00052-
595 06

596

Fig 1. Comparison of calibration beads and viruses using the CytoFLEX S and CytoFLEX nano.

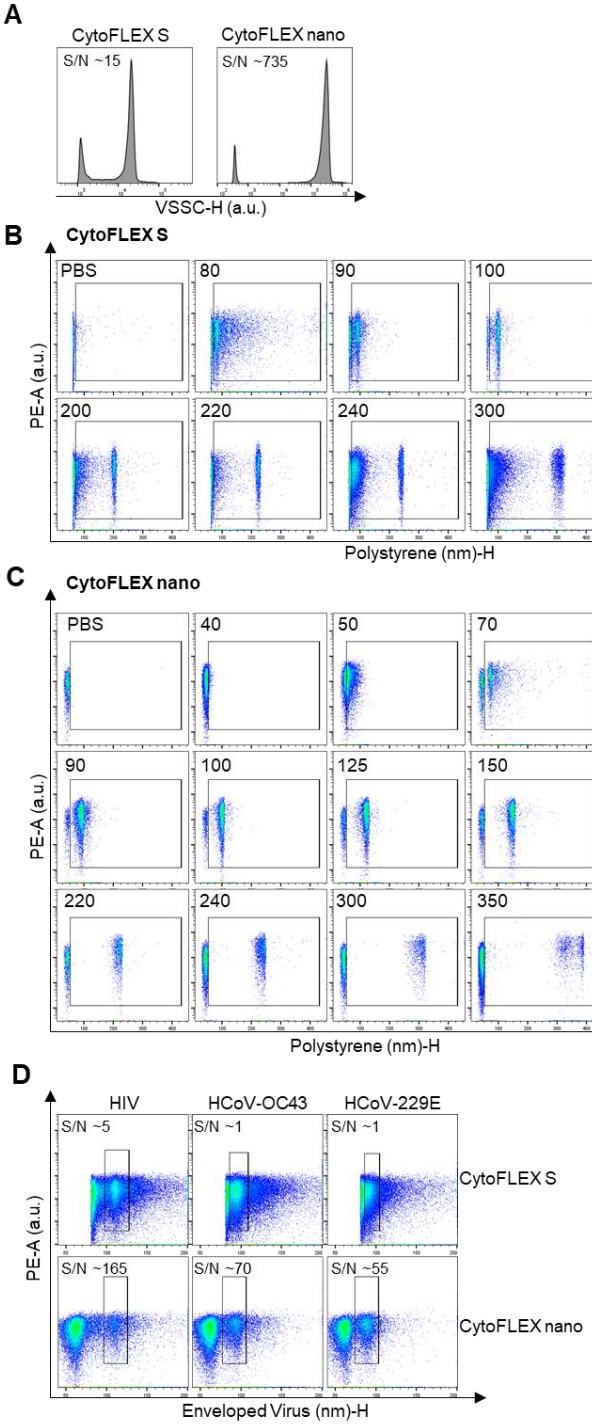

Figure 1. Comparison of calibration beads and viruses using the CytoFLEX S and CytoFLEX nano. (A) Detection of 100 nm polystyrene beads on the CytoFLEX S and CytoFLEX nano cytometers. Beads were resolved as distinct populations based on violet side scatter intensity (VSSC-H), with signal-to-noise ratios (S/N) indicated on the plots. Uncalibrated data are shown in arbitrary units (a.u.). (B) Pseudocolor dot plots for polystyrene beads ranging from 40 to 400 nm detected on the CytoFLEX S and (C) nano cytometers. Gates encompass the range of beads detected with scattering properties distinct from PBS. (D) Representative pseudocolor dot plots showing virus detection on both instruments, with S/N ratios indicated. Calibrated data are shown with enveloped virus sizing estimates generated through FCMPass using a refractive index of 1.456. Viral populations were identified by side scatter and are highlighted in the gated regions. Viral samples include HIV_{IIIB} and human coronaviruses (HCoVs), HCoV-OC43 and HCoV-229E.

Figure 2. Detecting host proteins on HIV virions.

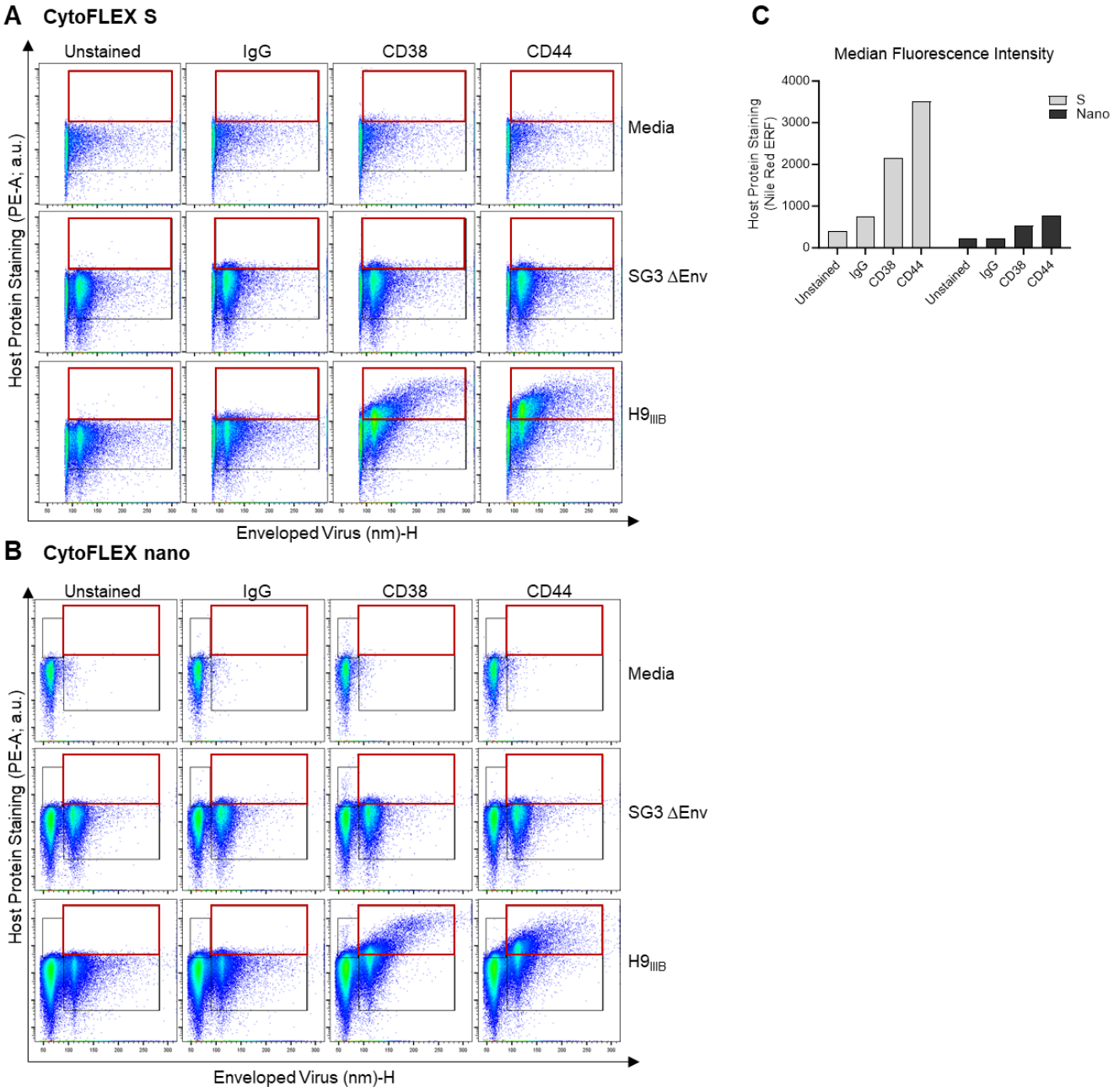

Figure 2. Detecting host proteins on HIV virions. (A-B) Presence of the cellular proteins CD38 and CD44 was assessed on HIV_{IIIB} virions produced in H9 cells ($H9_{IIIB}$) on the (A) CytoFLEX S or (B) CytoFLEX nano using PE-conjugated antibodies against the respective proteins. An isotype control antibody (IgG; targeting the irrelevant protein CD103) and unstained virus were used to assess nonspecific antibody binding and background fluorescence, respectively. HEK293T-derived pseudovirus, SG3 ΔEnv, is displayed as a negative virus control which lacks CD38 and CD44. Stained cell culture medium (DMEM) is shown to assess the contribution of antibodies in absence of virus to background fluorescence. In (A), the black gate is set based on the virus population as determined by scatter and is inclusive of the entire stained population, while the upper red gate denotes positive staining. In (B), the same gating strategy is shown as in (A), with an additional gate on the left of the x-axis set above instrument background fluorescence at the instrument threshold, which includes smaller particles including EVs and unbound antibody. (C) Median fluorescence intensity for the virus gate is shown for $H9_{IIIB}$ samples in calibrated equivalent reference fluorophore units (ERF) with Nile Red serving as the equivalent fluor for PE.

Fig 3. Comparing instrument utility for dual detection of host proteins on HIV.

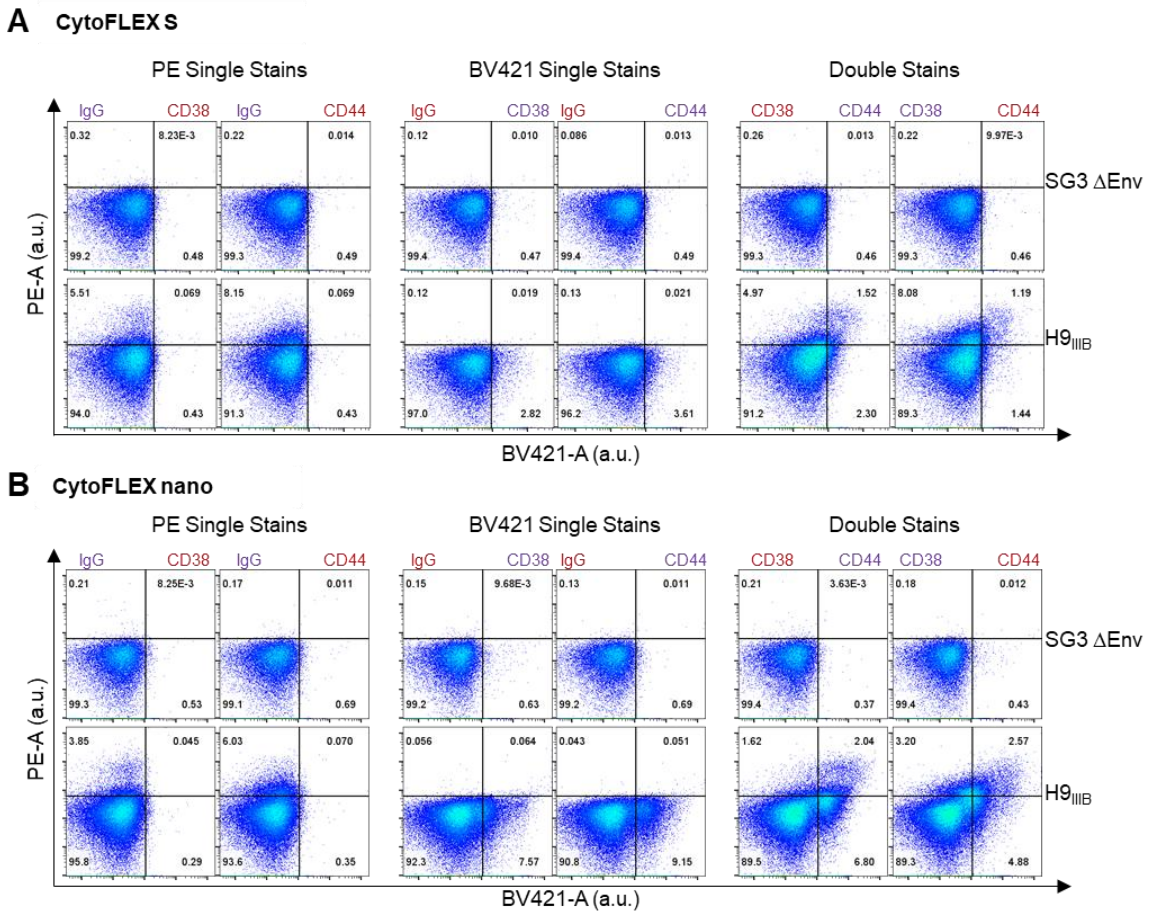

Fig 3. Comparing instrument utility for dual detection of host proteins on HIV. The presence of the cellular proteins CD38 and CD44 was assessed on $H9_{IIIB}$ virions on the (A) CytoFLEX S or (B) CytoFLEX nano using PE- and BV421- conjugated antibodies against the respective proteins. Isotype controls (IgG) were used to evaluate nonspecific staining for each channel. Red and purple labels represent PE- and BV421-labeled antibodies, respectively. The pseudovirus, SG3 ΔEnv is displayed as a virus control absent of CD38 and CD44. Gates are set based on staining with isotype controls on the SG3 ∆env virus stock.

Fig 4. Detecting tetraspanins on HIV virions.

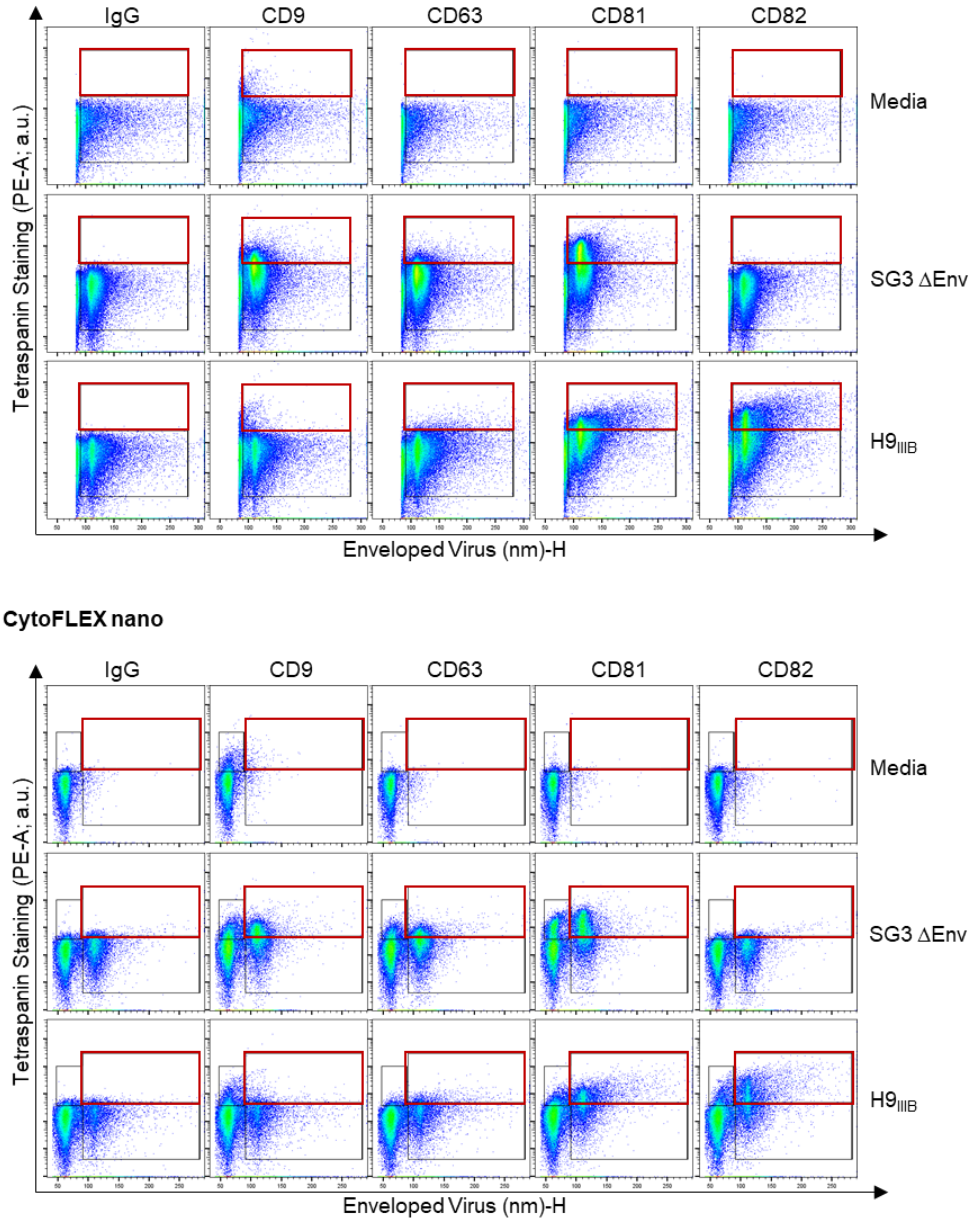

Fig 4. Detecting tetraspanins on HIV virions. Replication competent $H9_{IIIB}$ virions and SG3 ΔEnv pseudoviruses, were stained on the (A) CytoFLEX S or (B) CytoFLEX nano using PE- conjugated antibodies against tetraspanins (CD9, CD63, CD81, and CD82). An isotype control (IgG) is shown to assess nonspecific binding. A stained cell culture medium control is shown to assess contribution of antibodies alone (in absence of virus) to background fluorescence. In (A), the black gate is set based on the virus population as determined by scatter and is inclusive of the entire stained population, while the upper red gate denotes positive staining. In (B), the same gating strategy is shown as in (A), with an additional gate on the left of the x-axis set above instrument background fluorescence at the instrument threshold, which includes smaller particles including EVs and unbound antibody.

Fig 5. Evaluating presence of extracellular vesicles in HIV preparations.

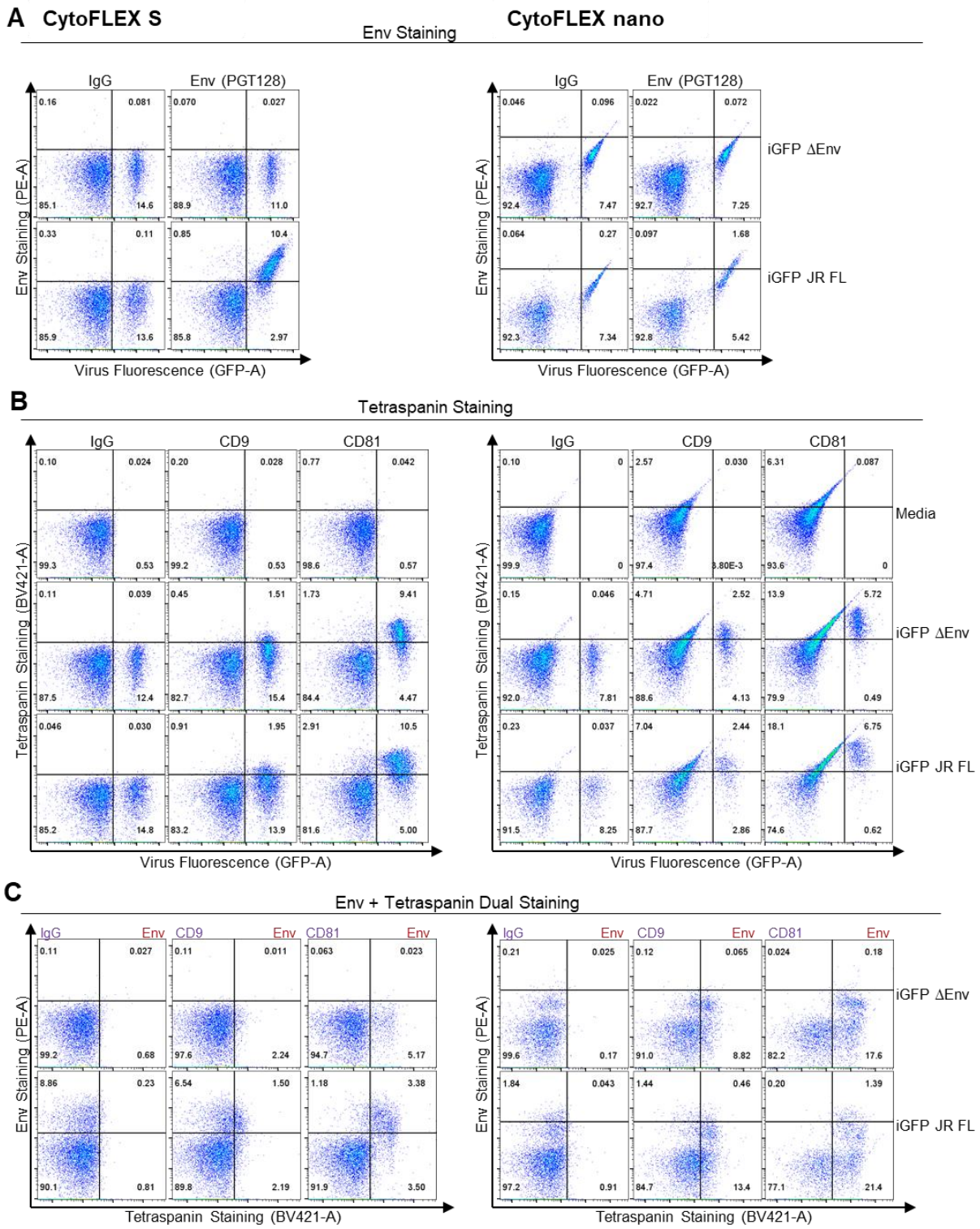

Fig 5. Evaluating presence of extracellular vesicles in HIV preparations. (A) Envelope glycoprotein staining was performed on the GFP-tagged infectious molecular clone iGFP, with or without (ΔEnv), the JR FL envelope. Samples were stained using either an isotype control or the anti-Env antibody PGT128, followed by detection with a PE-conjugated secondary antibody. Data were acquired on the CytoFLEX S (left panels) and the CytoFLEX nano (right panels). (B) Tetraspanin (CD9 and CD81) staining on viruses was performed using BV421-conjugated antibodies. Cell culture medium controls denote the contribution of antibodies alone to fluorescent signal. (C) Dual staining of HIV envelope glycoprotein and tetraspanins on HIV iGFP stocks. Gates are set based on staining with isotype controls on the ΔEnv virus stock. All fluorescence is displayed in arbitrary units.